◆ Human Brain Mapping 3:1–12(1995) ◆

Topography of Diprenorphine Binding in Human Cingulate Gyrus and Adjacent Cortex Derived From Coregistered PET and MR Images

Brent A. Vogt, Hiroshi Watanabe, Sylke Grootoonk, and Anthony K.P. Jones

Department of Physiology and Pharmacology, Bowman Gray School of Medicine, Wake Forest University, Winston-Salem, North Carolina (B.A.V.); Department of Investigative Radiology, National Cardiovascular Center Research Institute, Osaka, Japan (H.W.); Medical Research Council Clinical Sciences Centre, Royal Postgraduate Medical School, Hammersmith Hospital, London, United Kingdom (S.G.); Rheumatic Diseases Centre, Hope Hospital and University of Manchester, Salford, United Kingdom (A.K.P.J.)

Abstract: Positron emission tomography (PET) studies of ligand binding lack sufficient anatomical detail to evaluate topographical variations in binding within each of the lobes of the human cerebral cortex. This study employed PET to localize [^{11}C]diprenorphine binding to opioid receptors and magnetic resonance (MR) imaging for defining medial surface structures. Continuous arterial sampling for metabolite corrected [^{11}C]diprenorphine levels and CNS blood flow were used to model the volume of distribution (VD_{tot}) of binding for three subjects. The PET images of VD_{tot} were coregistered to the MR images for each case and 37 regions of interest were used to calculate VD_{tot}. The VD_{tot} was averaged for the three cases and coregistered with an MR reconstruction of the medial surface and plotted onto a flat map of this region.

The average VD_{tot} showed that binding was highest in anterior cingulate, rostral cingulofrontal transition, and prefrontal cortices, while binding in caudal parts of anterior cingulate and superior frontal cortices, and posterior cingulate cortex varied from high to low. Three statistical levels of binding were defined in relation to the high binding in perigenual area 24: high and equal to area 24, moderate and significantly lower than area 24 ($P < 0.01$), or low ($P < 0.001$). These levels of binding were plotted onto an unfolded map of the medial cortex. The VD_{tot} was high in rostral cortex, and a strip of high binding continued caudally on the dorsal lip of the cingulate gyrus. There were patches of high binding in cinguloparietal transition, posterior parietal, and supplementary motor cortices. Four regions had low binding: 1) areas 29 and 30 in the callosal sulcus, 2) fundus of the cingulate sulcus likely involving the cingulate motor areas, 3) fundus of the superior cingulate sulcus involving two divisions of supplementary motor cortex, and 4) sensorimotor cortex on the paracentral lobule. Variations in binding may reflect functional specializations such as low binding in the cingulate motor and visuospatial areas and high levels in areas involved in processing information with affective content. The higher sensitivity of three-dimensional scanning and coregistration of PET and MR images makes it feasible to analyze single individuals and, by performing pixel-by-pixel spectral analysis and generation of parametric maps, statistical analyses are possible.

Key words: flat map, opioid receptors, limbic cortex, cingulate cortex, frontal cortex, pain

INTRODUCTION

The actions of opiate drugs are exerted by opioid receptors throughout the CNS including the cerebral

Received for publication August 25, 1994; revision accepted May 5, 1995.

Address reprint requests to Brent A. Vogt, Department of Physiology and Pharmacology, Bowman Gray School of Medicine, Medical Center Boulevard, Winston-Salem, NC 27157-1083.

cortex. Morphine dissociates the functional components of the pain system. Thus, morphine blocks the affective features of acute and chronic noxious stimuli, while the sensory-discriminative component of pain remains intact [Price et al., 1985; Kupers et al., 1991]. One explanation for this dissociation is the high level of opioid binding in medial components of the pain system vs. low binding in the lateral pain system [Jones et al., 1991c]. In addition to reducing affective responses to pain, there is a long-latency elevation in mood (i.e., peak changes at about 2 hr) that follows morphine administration [Kaiko et al., 1981]. Thus, there are a number of actions of opiate compounds which are likely to be due to binding in different parts of the brainstem and cerebral cortex.

In experimental animals there are high levels of mu and delta opioid receptor binding in cortex on the medial surface of the hemisphere, including cingulate and frontal cortices, and moderate to low levels of kappa receptor binding [Mansour et al., 1987; Tempel and Zukin, 1987]. Opioid receptors have been localized to a number of afferent and intrinsic components of the cortical neuropil. Thus, opioid receptors regulate the release of noradrenaline in the cortex [Schoffelmeer and Mulder, 1982; Jackisch et al., 1986] and are expressed by thalamic axon terminals in the cortex [Vogt et al., 1992].

An early study of etorphine binding, which is mainly to mu receptors, in human brain in vitro showed high levels of binding in limbic cortical areas including anterior cingulate cortex [Hiller et al., 1973]. Ligand binding in vitro, however, is influenced by tissue incubation parameters such as the effect of sodium on agonist binding [Demoliou-Mason and Barnard, 1986], and may not reflect the topographical distribution of binding capacity in vivo. Diprenorphine, an opiate antagonist with similar affinities for the mu, delta, and kappa receptors in vivo, has high binding in anterior cingulate and prefrontal cortices [Jones et al., 1991c; Sadzot et al., 1991]. Furthermore, sensorimotor cortex has a low density of diprenorphine binding [Jones et al., 1991c]. In addition, carfentanil has a high affinity for mu opioid receptors and it also exhibits high binding in vivo in anterior cingulate and frontal cortices [Frost et al., 1990].

Besides localization of binding, imaging of opioid binding in vivo has been used as a means of assessing the functional state of cortical areas. Alterations in antagonist binding to opioid receptors can be used as a probe of cortical function, if one presumes that physiologically induced increases in the release of endogenous ligand displaces the binding of PET ligands to opioid receptors. Jones et al. [1994b] used PET imaging to examine [^{11}C]diprenorphine binding in individuals with rheumatoid arthritis who were in pain and following successful treatment of the pain. While in pain, these individuals had significantly reduced binding, possibly associated with elevated opioid levels, throughout much of the CNS including anterior cingulate, prefrontal, and orbitofrontal cortices. In this context, anatomical localization of ligand binding to specific parts of the cerebral cortex is particularly important.

The available human in vivo opiate binding studies have a number of limitations. Their limited spatial resolution precludes determining which particular cortical areas have high and low binding, and reconstruction of binding requires extrapolation among three reference planes. In addition, although distribution maps can be coregistered to structural scans in individuals, they employ color coding to denote binding patterns. Color coding can lead to misinterpretations about variations in binding, since these codes are not linearly related to binding capacity and grey scales cannot be coregistered to a black and white structural image.

The present study was undertaken to assess quantitative values of ligand binding using coregistered PET images for a number of individuals as well as coregistration of these images with magnetic resonance (MR) images. This approach provides a means of statistically evaluating binding in the cerebral cortex with a high degree of morphological resolution. Furthermore, a two-stage procedure for unfolding the medial cortical surface [Vogt et al., 1995] was used to render the distribution of binding on a flattened surface. This provided a more accurate means of assessing binding in the depths of the cerebral sulci. The strategy for this study included the following steps: 1) calculate [^{11}C]diprenorphine binding on a pixel-by-pixel basis for each case, 2) identify 37 regions of interest on the medial surface and calculate the binding capacity and its variance for PET to MR coregistered images for each case, 3) coregister PET binding data for the three cases and identify three statistical levels of significance for binding, and 4) coregister the three levels of binding onto parasagittal and coronal MR images and a flat map of a representative case. This latter step is not a volumetric calculation of binding, but rather an anatomical statement of heterogeneities in binding throughout the medial cortex. Finally, the approximate distribution of cortical areas was estimated from postmortem studies as a means of assessing variations of binding within different cortical areas in vivo and the possible functional consequences of heterogeneities in binding.

MATERIALS AND METHODS

MR imaging and flat map reconstruction

Subjects were three males aged 35, 46, and 53 with no history of neurological problems. Each individual received an MR scan with a 1 Tesla Picker HPQ Vista system using an RF spoiled volume acquisition that was relatively weighted to give good grey/white contrast and anatomical resolution (TR 24 ms; TE 6 ms; nonselective excitation with a flip angle of 35°; field of view in plane 25 × 25 cm; 192 × 256 in plane matrix with 128 secondary phase encoding steps oversampled to 256; resolution 1.3 × 1.3 × 1.5 mm; total imaging time 20 min). After reconstruction, the MR images were aligned parallel with the intercommissural line and interpolated to yield a cubic voxel size of 0.977 × 0.977 × 0.977 mm.

A two-stage flat-map technique has been used to assess the distribution of cytoarchitectural areas in Nissl-stained preparations [Vogt et al., 1995]. This approach was implemented to provide a single surface onto which variations in binding could be localized because much of the cortex is buried in the depths of sulci. Projecting cortical areas onto the convoluted brain, as originally done by Brodmann [1909], results in severe distortions of the topography of areas because all areas in the depths of the sulci must be shown on the gyral surface. Since [^{11}C]diprenorphine binding is heterogeneous, occurs in many parts of the cortex, and is difficult to interpret completely on a plane-by-plane basis, the flat-map technique was employed to render binding on the entire medial cortical surface.

The medial surfaces were reconstructed from 1 mm thick MR images. Since two of the cases had a double parallel pattern of cingulate sulci [Ono et al., 1990; Vogt et al., 1995], the sulcal pattern for a case with the double parallel pattern was used to reconstruct a flat map and for coregistration of the averaged PET image of binding. A drawing of the sulcal pattern on the medial surface was made to guide the reconstruction process as shown in Figure 1A. Reconstructions of the medial cortex are guided by the corpus callosum and the callosal sulcus which provide consistent landmarks for starting the flat map procedure. In terms of the surface features for this case there are two parallel cingulate sulci and two cingulate gyri. The ventral cingulate sulcus is continuous and terminates in the marginal ramus. One vertical branch of the cingulate sulcus rostral to the central sulcus is the paracentral sulcus. The parallel and segmented sulci rostral and dorsal to the anterior cingulate sulcus form the superior cingulate sulcus (the posterior segment of the cingulate sulcus of Ono et al. [1990]). The asterisk in Figure 1 denotes a rostral segment of the superior cingulate sulcus and there are three tissue bridges between the cingulate and superior cingulate sulci (short and straight arrows). The gyrus below the cingulate sulcus is the cingulate gyrus, while the gyrus between the cingulate and superior cingulate sulci is the superior cingulate gyrus. At the level of the marginal ramus in posterior cingulate cortex there are two vertical branches of the cingulate sulcus that extend into the cingulate gyrus. Caudal to the mar-

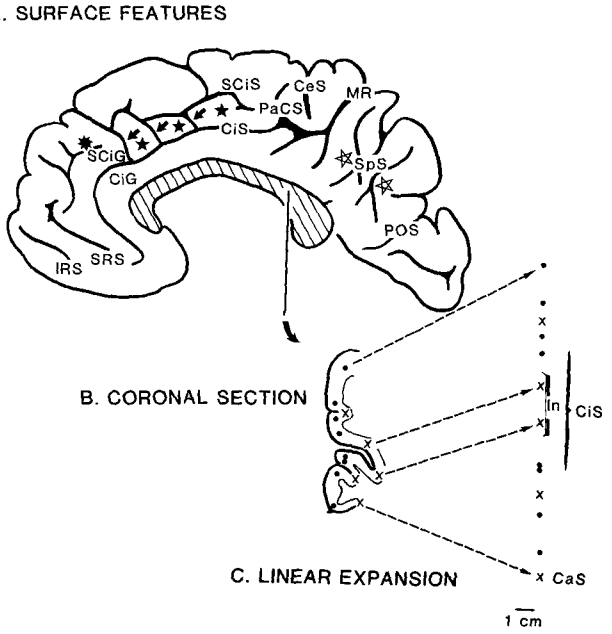

Figure 1.

Steps for the first stage of reconstructing a flat map of the medial surface. **A:** Line drawing of the surface features of the medial surface from a reconstruction of MR images. These sulci are identified: central sulcus (CeS); superior cingulate (SCiS) with its rostral segment (asterisk) and a branch forming the paracentral sulcus (PaCS); cingulate sulcus (CiS) with its marginal ramus (MR) and anastomoses (short straight arrows) with SCiS; inferior rostral sulcus (IRS); paracentral sulcus (PaCS); parietooccipital sulcus (POS); splenial sulci (SpS) and associated parasplenial lobules (two star outlines); superior rostral sulcus (SRS). The cingulate gyrus (CiG) and superior cingulate gyrus (SCiG) also are indicated. Segments of the SCiG are indicated with solid stars and the corpus callosum is cross hatched. **B:** Coronal section from posterior cingulate cortex with fiducials (dots for gyral apices and Xs for depths of sulci). In the depths of the CiS there is an insulette (*In*) marked by two Xs. **C:** Linear expansion of the fiducials beginning with the depths of the callosal sulcus (CaS) and including In which is bracketed.

ginal ramus is a highly branched splenial sulcus and associated parasplenial lobules.

For the first stage of flat map reconstruction every third 1 mm coronal MR image was used to place fiducial marks in the middle of the cortex (i.e., approximately between layers III or IV and V) at the apex of each gyrus and the fundus of each sulcus (Fig. 1B). The distances between the fiducials were measured with the depths of the callosal sulcus (CaS in Fig. 1C) as the origin and plotted onto graph paper. Occasionally there were cortical insulettes in the depths of the sulci ("In" in Fig. 1C) that were plotted onto the reconstruction to assure that the full cortical surface was represented. Linear expansions of all of the sections were aligned and points associated with the gyral apices and sulcal depths joined with solid and dashed lines, respectively.

The first stage of flattening does not take into account the fact that at places where there are prominent vertical sulci, such as the marginal ramus of the cingulate sulcus and the paracentral sulcus, there are distortions in the gyral surface area due to drawing the full depths of the sulcus. In other words, the volume of cortex on the gyral surface is particularly reduced at these points. The second stage of flattening involved extending the map rostrally and caudally at places where there were prominent vertical sulci. This was done by extending and rotating the corpus callosum ventrally so that there was a minimal amount of gyral surface extension. Dorsal areas on the superior frontal gyrus and posterior parietal areas are shifted posteriorally during the second stage of flattening. The second stage of flattening was repeated in a number of successive approximations in order to insure that there was minimal distortion of the cortex on both the gyral surface and sulcal depths. After each redrawing, the area of gyral surfaces was measured to see how closely they conformed to measurements taken from the surface feature map. This flat map was redrawn four times to approximate as closely as possible the extent of gyral surface features following the first linear extension.

Locations of cytoarchitectural areas on the medial surface for these studies were approximations based on observations of histological sections [Vogt et al., 1995]. In this latter study area 24 and the cingulofrontal transition area 32 were divided into rostral and caudal divisions (24/32 and 24′/32′, respectively). Areas 24, 24′, and 23 were separated into a ventral "a" division, a mid-gyral "b" division, and a sulcal "c" division. The primitive gigantopyramidal area of Braak [1976] was in the depths of the cingulate sulcus and was referred to as area 24c′g. In posterior cingulate cortex area 23 predominates with its three ventral-to-dorsal divisions: area 23a is aligned along the callosal sulcus, area 23b is dorsal to area 23a, and area 23c is in the depths of the cingulate sulcus. Retrosplenial cortex is in the depths of the callosal sulcus and includes areas 29 and 30. Finally, the cinguloparietal transition area 31 is located on the parasplenial lobules around the splenial sulcus. As an adjunct to evaluating the distribution of [^{3}H]diprenorphine binding, a figure is provided later in this article which has an approximate location for each of these areas (Fig. 5). No borders between areas can be provided, since the neuron architecture of areas in these subjects cannot be evaluated with current imaging techniques.

PET imaging and ligand binding modeling

Studies were performed on the ECAT 953B (Siemens/CPS, Knoxville, TN) brain tomograph system with 16 detector rings and retractable interplane collimators to allow acquisition of data in a high sensitivity, three-dimensional (3-D) mode. Data were reconstructed using the fully 3-D reconstruction to obtain images of the radioactivity distribution [Townsend et al., 1989] and that have transaxial resolution of 6 mm full width at half maximum at the center of the field-of-view (ramp filter, Nyquist cut off [Spinks et al., 1992]). In addition to increased sensitivity over the conventional acquisition mode, the 3-D mode of acquisition provides an increased acceptance of scattered events that need to be removed from the data to restore linearity of response to radioactivity concentrations and hence retain quantitation. After correction for the additional scattered events, the sensitivity gain is approximately fivefold [Spinks et al., 1992]. A dual energy window scatter correction was implemented where a fraction of a lower energy window data set was subtracted from the main upper energy window data set after smoothing to reduce the propagation of noise [Grootoonk et al., 1992]. For this purpose, all emission data were collected in two energy windows, and the emission data were corrected for scatter before reconstruction. The increased sensitivity of the 3-D acquisition mode combined with the correction and reconstruction methods allowed the generation of high quality, high resolution parametric images in single subjects [Tadokoro et al., 1993] which has obvious advantages over previously used methods of compartmental analysis of individual regions of interest [Jones et al., 1994a].

The axial extent of the scanner was 108 mm and scans were made with the tomograph aligned to the glabellar-inion line of the subjects to maximize the

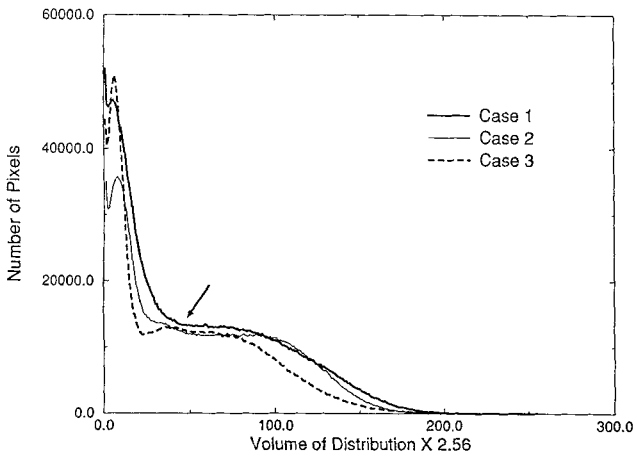

Figure 2.
Plots of the number of pixels for each VD_{tot} × 2.56 for the three cases. Values under 50 (arrow) are generally associated with activity in the white matter and CSF and were deleted from further analysis.

volume of brain viewed. A 20 min transmission scan was collected using external rotating ^{68}Ge rod sources to allow correction for attenuation of radioactivity in the tissue. The interplane collimators were then retracted and a 15 mCi bolus of [^{11}C]diprenorphine containing less than 10 μg unlabeled diprenorphine was injected intravenously and a 90 min emission scan was started simultaneously. This consisted of 17 dynamic time frames (6 × 3 min, 3 × 4 min, 4 × 5 min, 4 × 5 min) corresponding to 520 Mb of sinogram data that were reconstructed into 31 image planes. Intermittent blood samples were taken for measurement of whole blood/plasma ratios and plasma metabolites of diprenorphine [Jones et al., 1994a]. Plasma metabolites of diprenorphine were measured with solid phase extraction followed by HPLC so that a continuous plasma input function of unmetabolized [^{11}C]diprenorphine could be made. The spectral analysis technique was used to generate parametric images [Cunningham and Jones, 1993; Cunningham et al., 1991]. This technique provides a spectrum of the kinetic components which relate to the tissue and plasma time activity curves, and from which the unit impulse response function and volume of distribution of [^{11}C]diprenorphine binding (VD_{tot}) can be derived. The convolution of input and response functions gives the curve of best fit to the observed tissue data. The VD_{tot} for the three cases was multiplied by 2.56 because of the imaging format and to expand the scale of sensitivity and is shown in a histogram format for each case in Figure 2. Data points with a VD_{tot} below 50 were discarded because they are usually associated with binding in white matter and CSF. The arrow on Figure 2 delineates the low points that were discarded before the coregistration, statistical, and reconstruction procedures.

Coregistration of PET and MR images

The PET images of VD_{tot} for the three cases were coregistered on a pixel-by-pixel basis using an automated image realignment method [Woods et al., 1992]. This alignment algorithm calculates the ratio of one image to another at each voxel in the brain and then aligns the two images such that the variance of this ratio throughout all voxels is minimized. The algorithm includes the assumption that, if sets of two images are accurately aligned, the value of any voxel in one image set is related to the value of the corresponding voxel in the other image set by a single multiplicative factor. Coregistration of individual PET to MR images was accomplished for each case so that the VD_{tot} could be assessed in each of 37 ROI. The same Woods et al. [1992] method was used for this coregistration. During the coregistration procedure a histogram of the MR images was made and segmented for the realignment process. Once the PET and MR images had been coregistered, the original MRI data set was used for localizing binding to structures on the medial surface.

Statistical analysis

Artificial color codes are frequently used as a means of displaying the topographic distribution of binding in PET studies. Variations in the color scale, however, are misleading and often do not represent statistically significant variations. For example, color coding of the VD_{tot} values for [^{11}C]diprenorphine binding in the right and left hemispheres of these cases suggested that there were higher levels of binding in the nondominant hemisphere in each case. A statistical analysis of VD_{tot} for regions of interest in both hemispheres showed that no such differences exist. Thus, the right hemisphere was used from each case and is representative of the other hemisphere and color coding is only employed here to identify three levels of statistical significance.

Regions of interest (ROI) were specified for 37 cortical regions on the medial surface. The mean ± SEM VD_{tot} was calculated for each ROI for the three coregistered cases at each of the three parasagittal levels (Table I) and an ANOVA performed on values for the three levels. After this, the mean values for each ROI were calculated for all three parasagittal

TABLE I. Mean ± SEM VD_{tot} values for 37 regions of interest (ROI) on the medial surface calculated from coregistered PET and MR images for each case

ROI	"Area"	Level 1	Level 2	Level 3	ROI	"Area"	Level 1	Level 2	Level 3
1	25	139 ± 12	122 ± 4.9		20	10	138 ± 5.2	124 ± 16.8	
2	24a/b	132 ± 5.8			21	8	106 ± 17.9	95 ± 14.7	
3	24a/b	129 ± 6.1			22	6aβ	111 ± 11.9	117 ± 13.7	
4	24a/b	121 ± 7.2			23	6aα	101 ± 4.6	112 ± 6.7	
5	24b/c		105 ± 2.8		24	4	94 ± 11.2	93 ± 11.4	
6	24b/c		113 ± .61		25	23a/b	106 ± 1.7		
7	24b/c		115 ± 8.4		26	23a/b	98 ± 7.4		
8	24a'/b'	126 ± 6.8			27	23a/b	116 ± 6.1	102 ± 2.6	
9	24a'/b'	114 ± 3.6			28	23a/b	82 ± 5.5	91 ± 9.0	
10	24a'/b'	105 ± 5.8			29	23b/c		91 ± 9.7	
11	24b'/c'		107 ± 4.6		30	23b/c		106 ± 18.3	
12	24b'/c'		113 ± 18.4		31	23b			102 ± 172
13	24b'/c'		100 ± 11.7		32	23b			80 ± 4.4
14	24c			95 ± 4.0	33	23c			64 ± 18.3
15	24c'			73 ± 3.9	34	23c			97 ± 15.4
16	24c'			72 ± 14.4	35	31	103 ± 6.0	84 ± 12.8	
17	24c'g			66 ± 5.1	36	7m	100 ± 6.0	88 ± 10.5	83 ± 27.4
18	32	117 ± 11.4	115 ± 4.4	79 ± 6.7	37	17/18	42 ± 4.1	34 ± 3.7	33 ± 3.3
19	32'	123 ± 10.0	92 ± 17.2						

The three levels are parasagittal levels equivalent to those in Figure 3. The designations of the "areas" were approximations based on the corpus callosum and cingulate sulci. In some instances a single area occurs on more than one level.

levels (i.e., when an area was present in more than one parasagittal level, the VD_{tot} values were averaged for all levels; Table II). Subsequently, an orthogonal linear contrast was performed to assess the significance of differences among the 37 ROIs. The VD_{tot} for ROI 2, 3, and 4 are parts of perigenual area 24 and were used as the standard against which to test for significant variations in VD_{tot}. As discussed in the next section, three ranges of VD_{tot} were specified based on statistically significant differences and coregistered onto the medial surface MR image and the flat map rendering of the medial surface.

RESULTS

Binding in three-dimensional PET images

Three parasagittal MR images through the medial cortex at progressively more lateral levels are shown in Figure 3 (A,C,E). The first section is dominated by the gyral surface of the cingulate and superior frontal gyri, while the third section is dominated by cortex in the depths of the sulci including the cingulate sulci. On these levels are shown the 37 ROI. The mean ± SEM VD_{tot} for [^{11}C]diprenorphine binding was calculated for each ROI in the three coregistered cases (Table I). The highest levels of binding were in ROI in rostral cingulate areas 25 and 24, cingulofrontal transition areas 32 and rostral 32', and parts of frontal areas 6aβ, 8, and 10. Three levels of VD_{tot} were reconstructed onto the medial surface and coregistered onto the same MR images (Fig. 3B,D,F). Red codes for highest binding which was not different statistically from perigenual area 24 as discussed below. The highest binding was in anterior cingulate cortex including perigenual area 24 and area 25, cingulofrontal transition area 32, prefrontal cortex of the superior frontal gyrus including areas 10, 8, and 6aβ. Binding in posterior area 24 (i.e., area 24'), posterior cingulate cortex, the cinguloparietal transition region, and supplementary motor cortex was heterogeneous and best characterized with statistical and flat map methodologies.

Statistical testing was initiated with ANOVA for all ROI at each of the three parasagittal levels. Level 1 had an F statistic of 6.756 ($P < 0.0001$), level 2 had a value of 2.942 ($P < 0.002$), and level 3 had an F statistic of 2.202 ($P < 0.05$). Thus, there were significant variations in binding in all levels analyzed, although the most pronounced differences were between the gyral surfaces in anterior and posterior cingulate cortices. Since the ANOVA showed a significant level ($F = 35$, $P < 0.0001$) and ROI ($F = 5.12$, $P < 0.001$) effect, but not a level within ROI ($F = 0.81$, $P < 0.65$) effect, ROI

TABLE II. Combined VD_{tot} for each ROI and statistical analysis

ROI	Mean	Difference from 2–4	F	P	ROI	Mean	Difference from 2–4	F	P
2–4	127	—	—	—	20	131.2	4.2	0.19	—
1	130.5	3.5	0.14	—	21	100.5	−26.5	7.54	<.01
5	104.9	−22.1	3.29	—	22	114.8	−12.2	1.81	—
6	113.5	−13.5	1.22	—	23	106.5	−20.5	4.51	<.05
7	115.2	−11.8	0.93	—	24	93.7	−33.3	11.94	<.001
8	125.9	−1.1	0.01	—	25	105.9	−21.1	3.00	—
9	114.2	−12.8	1.10	—	26	98.2	−28.8	5.58	<.05
10	105.2	−21.8	3.19	—	27	109.0	−18.0	3.47	—
11	107.2	−19.8	2.64	—	28	86.9	−40.1	17.34	<.001
12	113.2	−13.8	1.28	—	29	90.9	−36.1	8.78	<.01
13	100.5	−26.5	4.71	<.05	30	106.5	−20.5	2.82	—
14	95.2	−31.8	6.80	<.05	31	102.5	−24.5	4.03	<.05
15	73.5	−53.5	19.24	<.001	32	80.2	−46.8	14.74	<.001
16	72.2	−54.8	20.21	<.001	33	64.2	−62.8	26.55	<.001
17	66.0	−61.0	21.61	<.001	34	97.5	−29.5	5.64	<.05
18	103.6	−23.4	7.27	<.01	35	93.5	−33.5	12.06	<.001
19	107.5	−19.5	4.08	<.05	36	90.4	−36.6	18.00	<.001
					37	36.5	−90.5	110.2	<.0001

Since differences in binding in areas at different levels were not significant, binding in each area was averaged across levels for each ROI. The mean value was tested for statistical significance in comparison to average binding in ROI 2–4 where binding was highest. The F and *P* values are given for each ROI and the dashed lines are for those regions that have the same level of binding as ROI 2–4.

was averaged across levels and an orthogonal linear contrast performed using the mean squared error for the entire sample. Table II gives the mean values for the averaged data, differences from the ROI 2–4, the F values, and *P* values for three levels of significance (dashed lines in Table II are for non-significant differences).

Binding in a flat map of the medial surface

The statistical analysis provides a format within which to evaluate binding in the unfolded map of the medial surface. A flat map is shown in Figure 4A where the nomenclature is the same as that in Figures 1 and 5. The cortical features that are shown in the flat map include the extensive cortical surface that is buried in the depths of the sulci. Along the fundus of the cingulate and superior cingulate sulci there are insulettes (i.e., small islands of cortex in the depths of the major sulci). To assist in interpreting this map, numbers 1–3 identify the apices of the following sulci: 1 = ventral border of the cingulate gyrus (the medial border of area 30), 2 = dorsal border of the cingulate gyrus that borders the ventral bank of the cingulate sulcus, 3 = dorsal border of the cingulate gyrus that borders the dorsal bank of the cingulate sulcus. The three straight arrows are the anastomoses between the cingulate and superior cingulate sulci, the asterisk identifies the rostral segment of the SCiS, and the solid stars indicate parts of the superior cingulate gyrus.

An anatomical representation of the distribution of [^{11}C]diprenorphine binding on the flat map was made by specifying the following ranges of VD_{tot} based on the above statistics: 1) 107–135, high and not different from ROI 2–4, 2) 95–106, moderate and significantly different from ROI 2–4 at $P < 0.05$–0.01, and 3) 35–94, low and significantly different from ROI 2–4 at $P < 0.001$. Each pixel for the averaged PET images was coded with red for high, white for moderate, and no color for low VD_{tot} as shown in Figure 3. These three densities of binding were reconstructed onto the flat map using the following information: 1) every third coronal image, 2) the three parasagittal levels in Figure 3, 3) a reconstruction of the binding from coronal images to the first stage linear reconstruction. Figure 4B shows the three levels of VD_{tot} reconstructed onto the flat map. Overall binding in anterior cingulate and prefrontal cortices was high as shown in the statistical analysis, however, binding in caudal anterior cingulate, posterior cingulate, supplementary motor, and parietal cortices was heterogeneous. A strip of high binding continued from anterior cingulate cortex into

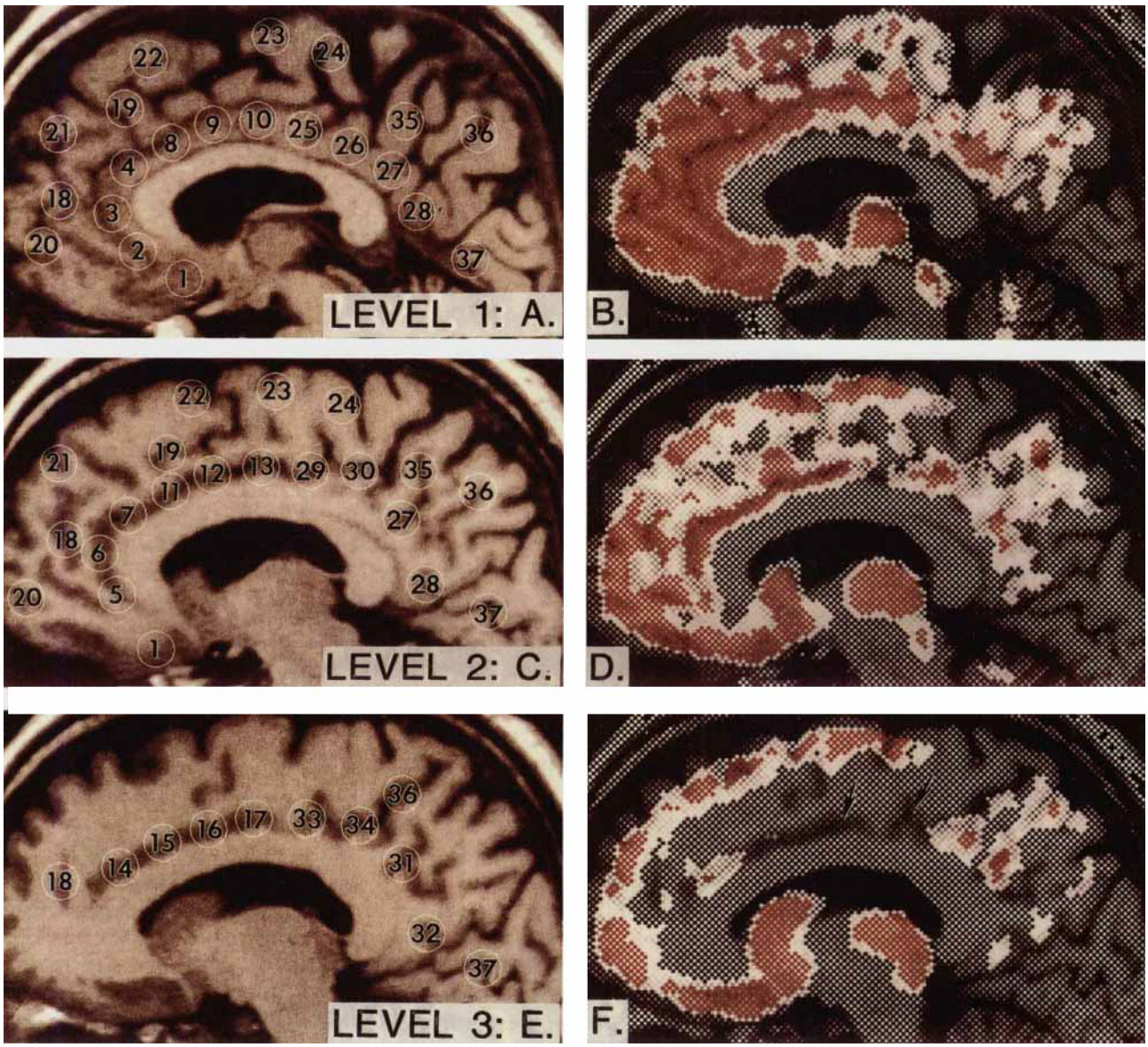

Figure 3.

Parasagittal MR images (**A,C,E**) and PET [^{11}C]diprenorphine binding (VD_{tot}) coregistered with MR (**B,D,F**) images through the medial surface. A/B are the most medial and include the gyral surface, while E/F are the most lateral and include mainly the sulcal depths. The numbers in each circle on the left are the ROI. The medial-lateral differences are associated with cortical areas on the gyral surface or in the depths of sulci. Color coding for PET images of [^{11}C]diprenorphine binding capacity is red for high, white for medium, and gray for low according to the statistical criteria. Binding in rostral anterior cingulate and prefrontal cortices was high, while binding in the depths of the cingulate sulcus was low-moderate (indicated with arrows in F).

area 24′ and the posterior cingulate gyrus. Notice that the three spots of high binding just dorsal to the cingulate sulcus are continuous with the ventral strip of binding when one views the cingulate sulcus as a closed structure instead of open as in the flat map.

In order to interpret the location of binding in terms of recent cytoarchitectural studies and relate differences in binding to cortical functions, Figure 5 is presented with an approximation of the locations of cytoarchitectural areas. Since the specific architecture of each area in these brains is not known, no borders are denoted in the diagram. These are meant as a guide for discussion of the approximate locations of areas on the medial surface. By referring to both

Figures 4 and 5 it can be seen that there were a number of patches of high binding in area 23b, the cingulo-parietal transition area 31, and posterior parietal area 7m. Binding in supplementary motor cortex on the superior frontal gyrus was significantly different in its two divisions. Area 6aα had moderate levels of binding, while area 6aβ had high binding.

There were four regions of low binding and each is numbered in Figure 4B. The first was in the depths of the callosal sulcus in areas 29 and 30. This area of low binding extended behind the corpus callosum and was continuous with primary and secondary visual areas. The second low binding region was in the fundus of the cingulate sulcus. Most binding in the depths of the cingulate sulcus was either low or moderate in density, although there was a short extension into the ventral bank of the cingulate sulcus. The depths of the cingulate sulcus contain the cingulate motor areas in areas 24c', 24c'g, and 23c. The third region of low binding was in the fundus of the superior cingulate sulcus and was likely to be associated with ventral parts of the supplementary motor areas 6aα and 6aβ. The fourth region of low binding surrounded the medial part of the central sulcus and extended rostrally into the paracentral sulcus and ventrally through the marginal ramus of the cingulate sulcus to include part of medial parietal cortex.

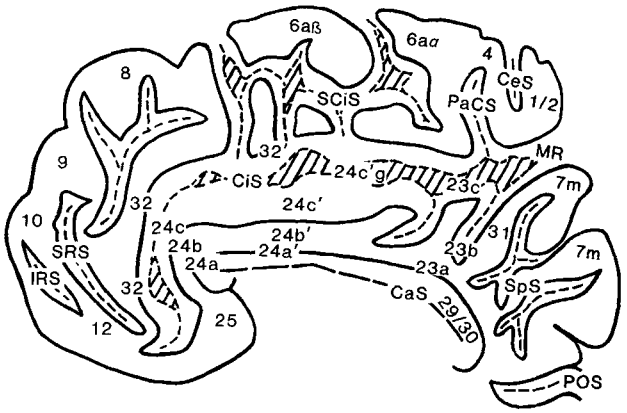

Figure 5.

The general location of cortical areas on the medial surface of the hemisphere to guide interpreting the pattern of [^{3}H]diprenorphine binding. Since the cytoarchitecture of areas is not known for the cases used in this study, their locations are approximations and no borders are delineated.

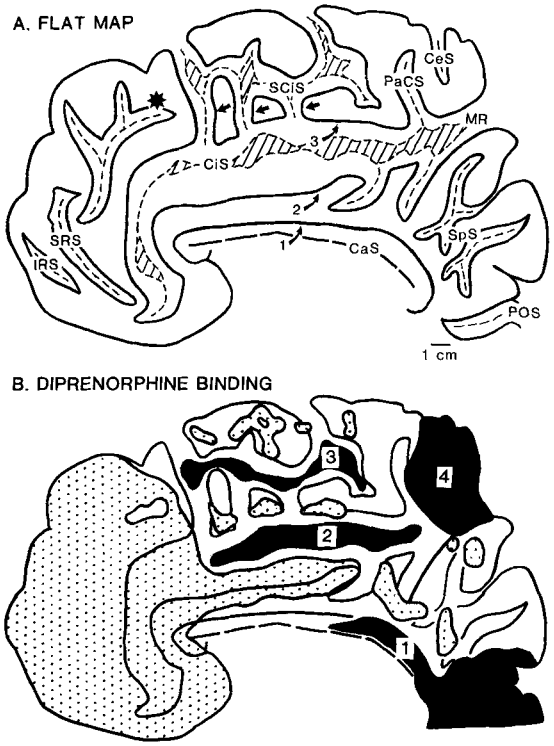

Figure 4.

A: Flat map reconstruction of one case which takes into account the full depths of the sulci (dashed lines) throughout the medial surface. Hatched areas in the depths of sulci are insulettes, and solid lines are the apices of gyral surfaces. The long-dashed lines are the depths of the callosal sulcus (CaS). Cortex between this and the first solid line is burried in the depths of the callosal sulcus. Other abbreviations are the same as in Figure 1. The curved arrows emphasize the boundaries of the cingulate gyrus: 1 is the ventral border of the cingulate gyrus, 2 is the dorsal border associated with the ventral bank of the cingulate sulcus, and 3 is the dorsal border of the cingulate gyrus that is associated with the dorsal bank of the cingulate sulcus. **B:** Reconstruction of VD_{tot} for [^{11}C]diprenorphine onto the flat map. The densities of binding are coded with dots for high, clear for moderate, and solid for low, with the latter numbered for reference in the text.

DISCUSSION

Diprenorphine binding on the medial surface of the hemisphere in anterior cingulate and frontal cortices was high as reported previously [Jones et al., 1991c; Sadzot et al., 1991]. The higher sensitivity of 3-D scanning and coregistration of PET to PET and PET to MR images enabled the present analysis of binding in individuals and, by performing pixel-by-pixel spectral analysis, the generation of parametric images for statistical analysis. Using these techniques along with a flat map derived from MR images, it was shown that diprenorphine binding in caudal parts of area 24, posterior cingulate cortex, supplementary motor cortex, and the cingulo-parietal transition region had striking heterogeneities. In addition, low binding oc-

curred in a number of regions including sensorimotor cortex, cortex in the depths of the cingulate sulci, and retrosplenial areas in the depths of the callosal sulcus. Variations in diprenorphine binding on the medial cortical surface suggest reasons for some of the actions of opiate compounds and may provide clues into the functional subdivisions of this region.

Part of anterior cingulate cortex is involved in pain processing and this region may be targeted by opiate compounds. Thus, noxious cutaneous stimulation elevates blood flow in middle parts of the cingulate gyrus [Jones et al., 1991a; Talbot et al., 1991; Casey et al., 1994] and neurosurgical cingulumotomies relieve chronic pain [Ballantine et al., 1967; Foltz and White, 1968; Devinsky and Luciano, 1993; Vogt et al., 1993]. A strip of high diprenorphine binding was noted in the present study that extended along the dorsal lip of the cingulate gyrus to area 24′ and likely included nociceptive cingulate cortex. Thus, opiate compounds can have a direct impact on aspects of pain processing that are mediated by anterior cingulate cortex.

Interestingly, much of the high diprenorphine binding in anterior parts of the medial surface may be rostral and dorsal to cortex that subserves pain processing. Since opiate compounds elevate mood in addition to regulating affective responses to pain [Lasagna et al., 1955; Kaiko et al., 1981], it is worth considering to what extent these anterior areas are involved in mood and other types of neuronal processing. First, morphine elevates blood flow in rostral and ventral parts of cingulate cortex including areas 24 and 25 [Jones et al., 1991b]. Second, some cases of major depression have reduced blood flow and glucose metabolism in anterior cingulate/cingulofrontal transition cortex [Bench et al., 1992; Wu et al., 1992]. Third, area 25 has been activated during self-induced sadness in healthy female subjects [George et al., 1995]. Thus, mood is likely an important adjunct to activity in anterior cingulate and cingulofrontal transition cortices and the high opiate binding in these areas is probably one reason for the mood-altering effects of opiate drugs.

Another function of anterior cingulate and frontal cortices is in cognitive processing [Devinsky et al., 1995]. These processes include response selection in a task of verb generation to unfamiliar lists of nouns [Raichle et al., 1994] and accessing declarative memory in verbal memory tasks [Grasby et al., 1993]. Although the role of opiate compounds in modulating these functions are not known, their binding in anterior parts of the medial surface of the hemisphere is likely to have an impact on cognitive processes.

Although the functions of each part of cingulate cortex are poorly understood, regions of low diprenorphine binding may be useful in identifying areas with a preponderance of sensorimotor functions as is true for lateral neocortical areas. There is evidence that parts of cingulate cortex are engaged in premotor function. Braak [1976] characterized a primitive gigantopyramidal area in the depths of the cingulate sulcus which is referred to here as area 24c′g. Subsequent primate studies have shown that a number of distinct cingulate regions project to the spinal cord [Biber et al., 1978; Dum and Strick, 1991] and contain neurons that have a long-lead time for skeletomotor activity [Shima et al., 1991]. These areas have been referred to as the cingulate motor areas [Dum and Strick, 1993]. Since diprenorphine binding was low in the depths of the cingulate sulcus as was the case for sensorimotor neocortex on the medial surface, it is likely that opiate compounds have little direct impact on corticospinal projection systems.

Supplementary motor cortex is composed of two areas on the medial surface (i.e., areas 6aα and 6aβ [Vogt and Vogt, 1919]). Each of these areas may have elevated blood flow during the performance of complicated finger movement sequences [Schlaug et al., 1994] and they appear to be structurally and functionally different in the monkey. Area 6aα is adjacent to area 4 and has a few Betz neurons in layer Vb and large layer IIIc pyramids, while area 6aβ does not have the Betz pyramids and has a more neuron dense layer IIIc (areas F3 and F6 of Matelli et al. [1991] are similar to areas 6aα and 6aβ, respectively). From a functional perspective, longer trains of electrical stimuli are required to evoke movements from area 6aβ than from area 6aα, the percentage of evoked movements increases during natural movements when stimulating area 6aβ, and the movements evoked from area 6aβ are generally slower and more natural than those evoked from area 6aα [Luppino et al., 1991]. Diprenorphine binding was different in each of these areas on the superior frontal gyrus, since it was high in area 6aβ and moderate in area 6aα. Thus, opiate compounds appear to have higher levels of binding in areas that are involved in the preparative and integrative processing of motor events.

Much of areas 23a and 23b had moderate levels of diprenorphine binding, while areas 29 and 30 had low binding capacity. These areas have been implicated in visuospatial functions with single unit recording in rabbit [Sikes et al., 1988], cat [Olson and Musil, 1992], and monkey [Olson et al., 1993] and with lesions in rat [Sutherland and Hoesing, 1993] and monkey [Murray et al., 1989]. In view of the moderate to low binding capacity for diprenorphine in these areas, opiate compounds should have limited impact on visuospa-

tial functions that are mediated by posterior cingulate cortex.

A combination of coregistration, statistical methods, and flat map rendering provides a high resolution means of displaying regional heterogeneities in ligand binding. This is a particularly important approach for studying in vivo binding in the human brain because about half of the cortical surface is buried in the depths of the sulci making the display of binding patterns difficult. The final solution to unfolding the convoluted surface of the human cerebral cortex will require computational algorithms. The qualitative approach used here, however, provides a first approximation of the flattened medial surface and raises issues that should be considered when developing computational solutions. It also serves as the basis for understanding opiate regulation of specific functions subserved by medial cortical structures.

ACKNOWLEDGMENTS

We thank Drs. Robert Hampson and Stuart Derbyshire for their assistance with the statistical analysis. Funding for these studies was provided by the United Kingdom Medical Research Council, the Burroughs Wellcome Fund, and the British Medical Association.

REFERENCES

Ballantine HT, Cassidy WL, Flanagan NB, Marino R Jr (1967): Stereotaxic anterior cingulotomy for neuropsychiatric illness and intractable pain. J Neurosurg 26:488–495.

Bench CJ, Friston KJ, Brown RG, Scott LC, Frackowiak RSJ, Dolan RJ (1992): The anatomy of melancholia-focal abnormalities of cerebral blood flow in major depression. Psychol Med 22:607–615.

Biber MP, Kneisley LW, LaVail JH (1978): Cortical neurons projecting to the cervical and lumbar enlargements of the spinal cord in young and adult rhesus monkey. Exp Neurol 59:492–508.

Braak H (1976): A primitive gigantopyramidal field buried in the depth of the cingulate sulcus of the human brain. Brain Res 109:219–233.

Brodmann K (1909): Vergleichende Lokalisationslehre der Grosshirnrinde in ihren Prinzipien dargestellt auf Grund des Zellenbaues. Leipzig: Barth.

Casey KL, Minoshima S, Berger KL, Koeppe RA, Morrow TJ, Frey KA (1994): Positron emission tomographic analysis of cerebral structures activated specifically by repetitive noxious heat stimuli. J Neurophysiol 71:802–807.

Cunningham VJ, Jones T (1993): Spectral analysis of dynamic PET studies. J Cereb Blood Flow Metab 13:15–23.

Cunningham VJ, Fujiwara T, Luthra SK, Jones T, Jones AKP (1991): A procedure and compartmental analysis for measuring cerebral kinetics of ^{11}C-diprenorphine in man. J Cereb Blood Flow Metab 2:S619.

Demoliou-Mason CD, Barnard EA (1986): Distinct subtypes of the opioid receptor with allosteric interactions in brain membranes. J Neurochem 46:1118–1128.

Devinsky O, Luciano D (1993): The contributions of cingulate cortex to human behavior. In: Vogt BA, Gabriel M (eds): Neurobiology of Cingulate Cortex and Limbic Thalamus. Boston: Birkhäuser, pp 527–556.

Devinsky O, Morrell MJ, Vogt BA (1995): Contributions of anterior cingulate cortex to behavior. Brain 118:279–306.

Dum RP, Strick PL (1991): The origin of corticospinal projections from the premotor areas in the frontal lobe. J Neurosci 11:667–689.

Dum RP, Strick PL (1993): Cingulate motor areas. In: Vogt BA, Gabriel M (eds): Neurobiology of Cingulate Cortex and Limbic Thalamus. Boston: Birkhäser, pp 415–441.

Foltz EL, White LE (1968): The role of rostral cingulumotomy in "pain" relief. Int J Neurol 6:353–373.

Frost J, Mayberg HS, Sadzot B, Dannals RF, Lever JR, Ravert HT, Wilson AA, Wagner Jr HN, Links JM (1990): Comparison of [^{11}C]diprenorphine and [^{11}C]carfentanil binding to opiate receptors in humans by positron emission tomography. J Cereb Blood Flow Metab 10:484–492.

George MS, Ketter TA, Parekh PI, Horwitz B, Herscovitch P, Post RM (1995): Brain activity during transient sadness and happiness in healthy women. Am J Psychiatry 152:341–351.

Grasby PM, Frith CD, Friston KJ, Bench C, Frackowiak RSJ, Dolan RJ (1993): Functional mapping of brain areas implicated in auditory-verbal memory function. Brain 116:1–20.

Grootoonk S, Spinks TJ, Jones T, Michel C, Bol A (1992): Correction of scatter using a dual energy window technique with a tomograph operated without septa. 1991 IEEE Medical Imaging Conf Rec 3:1569–1573.

Hiller JM, Pearson J, Simon EJ (1973): Distribution of stereospecific binding of the potent narcotic analgesic etorphine in the human brain: Predominance in the limbic system. Res Comm Chem Pathol Pharmacol 6:1052–1062.

Jackisch R, Geppert M, Illes P (1986): Characterization of opioid receptors modulating noradrenaline release in the hippocampus of the rabbit. J Neurochem 46:1802–1810.

Jones AKP, Brown WD, Friston KJ, Qi LY, Frackowiak RSJ (1991a): Cortical and subcortical localization of response to pain in man using positron emission tomography. Proc R Soc London, Ser B, 244:39–44.

Jones AKP, Friston KJ, Qi LY, Harris M, Cunningham VJ, Jones T, Feinman C, Frackowiak RSJ (1991b): Sites of action of morphine in the brain. Lancet 338:825.

Jones AKP, Qi LY, Fujirawa T, Luthra SK, Ashburner J, Bloomfield P, Cunningham VJ, Itoh M, Fukuda H, Jones T (1991c): In vivo distribution of opioid receptors in man in relation to the cortical projections of the medial and lateral pain systems measured with positron emission tomography. Neurosci Lett 126:25–28.

Jones AKP, Cunningham VJ, Ha-Kawa SK, Fujiwara T, Qi L, Luthra SK, Ashburner J, Osman S, Jones T (1994a): Quantitation of ^{11}C-diprenorphine cerebral kinetics in man acquired by PET using presaturation, pulse-chase and tracer alone protocols. J Neurosci Methods 51:123–134.

Jones AKP, Qi L, Cunningham VJ, Ha-Kawa SK, Fujirawa T, Luthra SK, Silva S, Derbyshire S, Jones T (1994b): Changes in central opioid receptor binding in relation to inflamation and pain in patients with rheumatoid arthritis. Br J Rheumatol, 33:909–916.

Kaiko RF, Wallenstein SL, Rogers AG, Grabinski PY, Houde RW (1981): Analgesic and mood effects of heroin and morphine in cancer patients with postoperative pain. New Engl J Med 304:1501–1505.

Kupers RC, Konings H, Adriaensen H, Gybels JM (1991): Morphine differentially affects the sensory and affective pain ratings in neurogenic and ideopathic forms of pain. Pain 47:5–12.

Lasagna L, von Felsinger JM, Beecher HK (1955): Drug-induced mood changes in man. JAMA 157:1006–1020.

Luppino G, Matelli M, Camarda RM, Gallese V, Rizzolatti G (1991): Multiple representations of body movements in mesial area 6 and the adjacent cingulate cortex: An intracortical microstimulation study in the macaque monkey. J Comp Neurol 311:463–482.

Mansour A, Khachaturian H, Lewis ME, Akil H, Watson SJ (1987): Autoradiographic differentiation of mu, delta, and kappa opioid receptors in the rat forebrain and midbrain. J Neurosci 7:2445–2464.

Matelli M, Luppino G, Rizzolatti G (1991): Architecture of superior and mesial area 6 and the adjacent cingulate cortex in the macaque monkey. J Comp Neurol 311:445–462.

Murray EA, Davidson M, Gaffan D, Olsoen DS, Suomi S (1989): Effects of fornix transection and cingulate cortical ablation on spatial memory in rhesus monkeys. Exp Brain Res 74:173–186.

Olson CR, Musil SY (1992): Sensory and oculomotor functions of single neurons in the posterior cingulate cortex of cats. Cereb Cortex 2:485–502.

Olson CR, Musil SY, Goldberg ME (1993): Posterior cingulate cortex and visuospatial cognition: Properties of single neurons in the behaving monkey. In: Vogt BA, Gabriel M (eds): Neurobiology of Cingulate Cortex and Limbic Thalamus. Boston: Birkhäuser.

Ono M, Kubik S, Abernathey CD (1990): Atlas of the Cerebral Sulci. New York: Thieme Medical Publishers, Inc.

Price DD, Von der Gruen A, Miller J, Rafii A, Price C (1985): A psychophysical analysis of morphine analgesia. Pain 22:261–269.

Raichle ME, Fiez JA, Videen TO, MacLeod A-MK, Pardo JV, Fox PT, Petersen SE (1994): Practice-related changes in human brain functional anatomy during nonmotor learning. Cereb Cortex 4:8–26.

Sadzot B, Price JC, Mayberg HS, Douglass KH, Dannals RF, Lever JR, Ravert HT, Wilson AA, Wagner HN, Feldman MA, Frost JJ (1991): Quantification of human opiate receptor concentration and affinity using high and low specific activity [^{11}C]diprenorphine and positron emission tomography. J Cereb Blood Flow Metabol 11:204–219.

Schlaug G, Knorr U, Seitz RJ (1994): Inter-subject variability of cerebral activations in acquiring a motor skill: A study with positron emission tomography. Exp Brain Res 98:523–534.

Schoffelmeer ANM, Mulder AH (1982): Presynaptic α-adrenoceptors and opiate receptors: Inhibition of [^{3}H]noradrenaline release from rat cerebral cortex slices by different mechanisms. Eur J Pharmacol 79:329–332.

Sikes RW, Vogt BA, Swadlow HA (1988): Neuronal responses in rabbit cingulate cortex linked to quick-phase eye movements during nystagmus. J Neurophysiol 59:922–936.

Shima K, Aya K, Mushiake H, Inase M, Aizawa H, Tanji J (1991): Two movement-related foci in the primate cingulate cortex observed in signal-triggered and self-paced forelimb movements. J Neurophysiol 65:188–202.

Spinks TJ, Jones T, Bailey DL, Townsend DW, Grootoonk S, Bloomfield PM, Gilardi MC, Casey ME, Sipe B, Reed J (1992): Physical performance of a positron tomograph for brain imaging with retractable septa. Phys Med Biol 37:1637–1655.

Sutherland RJ, Hoesing JM (1993): Posterior cingulate cortex and spatial memory: A microlimnology analysis. In: Vogt BA, Gabriel M (eds): Neurobiology of Cingulate Cortex and Limbic Thalamus. Boston: Birkhäuser.

Tadokoro M, Jones AKP, Cunningham VJ, Sashin D, Grootnoonk S, Ashburner J, Jones T (1993): Parametric images of ^{11}C-diprenorphine binding using spectral analysis of dynamic PET images acquired in 3-D. In: Uemura K (ed): Quantitation of Brain Function, Tracer Kinetics and Image Analysis in Brain PET. Amsterdam: Elsevier Science Publishers B.V., pp 289–294.

Talbot JD, Marrett S, Evans AC, Meyer E, Bushnell MC, Duncan GH (1991): Multiple representations of pain in human cerebral cortex. Science 251:1355–1358.

Tempel A, Zukin RS (1987): Neuroanatomical patterns of the μ, δ, and k opioid receptors of rat brain as determined by quantitative in vitro autoradiography. Proc Natl Acad Sci USA 84:4308–4312.

Townsend DW, Spinks TJ, Jones T, Geissbuhler A, Defrise M, Gilardi MC, Heather J (1989): Fully three-dimensional reconstruction for a PET camera with retractable septa. Eur J Nucl Med 15:741–745.

Vogt BA, Crino PB, Jensen EL (1992): Multiple heteroreceptors on limbic thalamic axons: M_2 acetylcholine, serotonin$_{1B}$, beta$_2$ adrenoceptors, mu opioid and neurotensin. Synapse 10:44–53.

Vogt BA, Sikes RW, Vogt LJ (1993): Anterior cingulate cortex and the medial pain system. In: Vogt BA, Gabriel M (eds): Neurobiology of Cingulate Cortex. Boston: Birkhäuser, pp 313–344.

Vogt BA, Nimchinsky E, Vogt LJ, Hof P (1995): Human cingulate cortex: Surface features, flat maps, and cytoarchitecture. J Comp Neurol, 359:490–506.

Vogt C, Vogt O (1919): Allgemeinere ergebnisse unserer Hirnforschung. J Psychol Neurol (Leipzig) 25:277–462.

Wamsley JK, Zarbin MA, Young WS, Kuhar MJ (1982): Distribution of opiate receptors in the monkey brain: An autoradiographic study. Neuroscience 7:595–613.

Woods RP, Cherry SR, Maziortta JC (1992): A rapid autimated algorithm for accurately aligning and reslicing PET images. J Comput Assist Tomogr 16:620–633.

Wu JC, Gillin JC, Buchsbaum MS, Hershey T, Johnson JC, Bunney Jr WF (1992): Effect of sleep deprivation on brain metabolism of depressed patients. Am J Psychiatry 149:538–543.